INTERNATIONAL JOURNAL FOR NUMERICAL METHODS IN FLUIDS
Int. J. Numer. Meth. Fluids 2009; **60**:691–708
Published online 17 September 2008 in Wiley InterScience (www.interscience.wiley.com). DOI: 10.1002/fld.1913

Lattice Boltzmann method for flows in porous and homogenous fluid domains coupled at the interface by stress jump

Huixing Bai[1], P. Yu[1], S. H. Winoto[1] and H. T. Low[2,*,†,‡]

[1]*Department of Mechanical Engineering, National University of Singapore, 9 Engineering Drive 1, Singapore 117576, Singapore*
[2]*Division of Bioengineering Engineering, National University of Singapore, 9 Engineering Drive 1, Singapore 117576, Singapore*

SUMMARY

A numerical method was developed for flows involving an interface between a homogenous fluid and a porous medium. The numerical method is based on the lattice Boltzmann method for incompressible flow. A generalized model, which includes Brinkman term, Forcheimmer term and nonlinear convective term, was used to govern the flow in the porous medium region. At the interface, a shear stress jump that includes the inertial effect was imposed for the lattice Boltzmann equation, together with a continuity of normal stress. The present method was implemented on three cases each of which has a porous medium partially occupying the flow region: channel flow, plug flow and lid-driven cavity flow. The present results agree well with the analytical and/or the finite-volume solutions. Copyright © 2008 John Wiley & Sons, Ltd.

Received 13 February 2008; Revised 29 July 2008; Accepted 29 July 2008

KEY WORDS: interfacial boundary condition; stress jump; porous medium; lattice Boltzmann method

1. INTRODUCTION

The study of flow systems, which is composed of porous media and homogenous fluids, has attracted considerable attention since they occur in a wide range of the industrial and environmental applications. Examples of practical applications are bioreactors with porous scaffolds, drug delivery with porous microspheres, fuel cells, drying process, electronic cooling and ceramic processing. To solve this type of problems, there are three different approaches: the domain scale approach, the representative elementary volume (REV) scale approach and the pore scale approach.

*Correspondence to: H. T. Low, Division of Bioengineering Engineering, National University of Singapore, 9 Engineering Drive 1, Singapore 117576, Singapore.
†E-mail: mpelowht@nus.edu.sg
‡Associate Professor.

In the domain scale approach, the composite region is considered as a continuum and one set of general governing equations is applied for the whole domain [1–5]. The explicit formulation of boundary condition is avoided at the interface and the transitions of the properties between the fluid and porous medium are achieved by certain artifacts [5]. Although this method is relatively easy to implement, the flow behavior at the interface depends on how the code is structured [6].

In the REV scale approach, two sets of governing equations are applied to describe the flow in the two regions and additional boundary conditions are applied at the interface to couple the two sets of equations. The interfacial boundary conditions at the porous–fluid interface are summarized in Table I.

The earliest study on the interfacial conditions is that by Beavers and Joseph [7]. In their approach, the flows in a homogenous fluid and a porous medium are governed by the Navier–Stokes and Darcy equations, respectively. The governing equations are of different orders in different regions. Thus a semi-empirical slip boundary condition was proposed at the interface to couple the equations. To make the governing equations of the same order, Neale and Nader [8] introduced the Brinkman term in the Darcy equation for the porous medium. The continuity of both stress and velocity was proposed at the interface. An analytical solution of this model was deduced by Vafai and Kim [9]. Another interfacial boundary condition involving continuous stress was proposed by Kim and Choi [10] who used the effective viscosity in the porous medium.

Later, Ochoa-Tapia and Whitaker [11, 12] deduced a stress jump condition at the interface based on the non-local form of the volume-averaged method. The stress jump condition means that, at the interfacial boundary, there is continuity of the volume-averaged velocity but the volume-averaged velocity profile has a change of slope. One of the strong points of such a boundary condition is that the jump is based on the stress but not on the velocity, and this has important consequences for heat and mass transfer processes since it allows the convective transport to be continuous at the fluid–porous interface boundary [11]. By adding the Forchheimer term to the Brinkman extended

Table I. Interface boundary conditions between porous medium and homogenous fluid domains.

Model	Velocity	Velocity gradient	Reference
1		$\left.\frac{\partial u_x}{\partial y}\right\|_{\text{fluid}} = \frac{\alpha}{\sqrt{K}}(u_x\|_{\text{interface}} - \langle u\rangle_\infty)$	[7]
2	$\langle u\rangle_x\|_{\text{porous}} = u_x\|_{\text{fluid}}$	$\left.\frac{\partial\langle u\rangle_x}{\partial y}\right\|_{\text{porous}} = \left.\frac{\partial u_x}{\partial y}\right\|_{\text{fluid}}$	[8, 9]
3	$\langle u\rangle_x\|_{\text{porous}} = u_x\|_{\text{fluid}}$	$v_e\left.\frac{\partial\langle u\rangle_x}{\partial y}\right\|_{\text{porous}} = v\left.\frac{\partial u_x}{\partial y}\right\|_{\text{fluid}}$	[10]
4	$\langle u\rangle_x\|_{\text{porous}} = u_x\|_{\text{fluid}}$	$\frac{1}{\varepsilon}\left.\frac{\partial\langle u\rangle_x}{\partial y}\right\|_{\text{porous}} - \left.\frac{\partial u_x}{\partial y}\right\|_{\text{fluid}} = \left.\frac{\beta}{\sqrt{K}}u_x\right\|_{\text{interface}}$	[11, 12]
5	$\langle u\rangle_x\|_{\text{porous}} = u_x\|_{\text{fluid}}$	$\frac{1}{\varepsilon}\left.\frac{\partial\langle u\rangle_x}{\partial y}\right\|_{\text{porous}} - \left.\frac{\partial u_x}{\partial y}\right\|_{\text{fluid}} = \left.\frac{\beta}{\sqrt{K}}u_x\right\|_{\text{interface}} + \left.\frac{\beta_1}{v}u_x^2\right\|_{\text{interface}}$	[13]

DOI: 10.1002/fld

Darcy equation for porous medium, Ochoa-Tapia and Whitaker [13] developed another stress jump condition, which includes the inertial effects. Two coefficients appear in this jump condition: one is associated with an excess viscous stress and the other is related to an excess inertial stress.

The implementation of the numerical methodology on the stress jump condition based on Ochoa-Tapia and Whitaker [11, 12] can be found in the work of Silva and de Lemos [3]. They used the finite-volume method with an orthogonal Cartesian coordinate system, which is not easy to apply for complex geometries. The jump in shear stress was considered and there was no special treatment on velocity derivatives. Alazmi and Vafai [14] proposed different types of interfacial conditions between a porous medium and a homogenous fluid and found that interfacial conditions have pronounced effects on the velocity field.

Recently, Yu *et al.* [15] developed a numerical method based on finite-volume method with a collocated variable arrangement to treat the stress jump condition given by Ochoa-Tapia and Whitaker [13], which includes the inertial effects. Yu *et al.* [15] used body-fitted and multi-block grids to treat the fluid and porous regions. Their method is effective for the coupled problems in homogenous fluid and porous medium regions with complex geometries.

Besides the computational fluid dynamics (CFD) models based on the momentum equations, a relatively new approach to model porous medium flows is based on the lattice Boltzmann equations (LBEs). Martys [16] used the lattice Boltzmann method (LBM) to model the flow through and over a partial porous medium in a channel. The study assumed continuation of both velocity and shear stress at the interface, by defining an effective viscosity term. The Stokes and Brinkman equations were used for fluid and porous flow, respectively. Through a Chapmann–Enskog procedure, these governing equations can be transformed into LBE. A body force term caused by the porous medium was incorporated into the LBE as a linear first-order or second-order Hermite polynomials. Later, Guo and Zhao [17] extend the study by using the generalized Navier–Stokes equation and Darcy–Brinkman–Forchheimer equation for the fluid and porous medium, respectively. They also assumed continuation of both velocity and shear stress at the interface using the effective viscosity. In their study, the porosity was included into the equilibrium distribution function (EDF), and a body force term was added to the LBE to account for the linear and nonlinear drag forces caused by the porous medium.

The main advantage of the LBM is that it is capable of resolving micro-physical and micro-chemical processes as demonstrated by Pan *et al.* [18] and Wang *et al.* [19]. At the pore scale, there is no requirement for special treatment of the shear stress jump at the interface. However, the LBM implementation at the pore scale for heterogenous porous media needs detailed geometric information and very large lattice sizes [17–19]. The current computer resources may be sufficient to resolve the pore scale for both the LBM and CFD in two-dimensional cases. However, in three-dimensional cases especially for larger flow systems, the REV scale methods have an advantage. As compared with the traditional CFD, the REV scale methods in the LBM framework have the following strong points [16, 17]: easy to implement, computationally efficient, natural for parallel computing and easy to treat complicated boundary. Thus, the present method is based on the REV scale and implemented in the LBM framework for two-dimensional cases. For future work, it will be useful if the present method can be demonstrated for three-dimensional cases.

In the existing LBM models for coupled flow with fluid and porous media, the assumed boundary condition is based on the continuation of shear stress at the interface through the use of the effective viscosity. However, as described earlier, there are other suitable boundary conditions, for example, the stress jump conditions. It would be of interest to examine how the stress jump conditions can be incorporated into the LBM model.

DOI: 10.1002/fld

The purpose of this paper is to extend the LBM for coupled problems of a fluid layer and porous medium layer, by using the stress jump interfacial boundary conditions. The treatments of both the velocity and distribution functions (DFs) at the interface are described. To study the viscous and inertial effects, the lattice Boltzmann models [17] for Navier–Stokes equation and Darcy–Brinkman–Forchheimer equation, with incompressibility assumption, are used in this paper.

2. GOVERNING EQUATIONS AND BOUNDARY CONDITIONS

The governing equations for porous medium flow based on Darcy–Brinkman–Forchheimer extended model are expressed in the vector form [15, 17]

$$\nabla \cdot \mathbf{u} = 0 \tag{1}$$

$$\underbrace{\nabla \cdot \left(\frac{\mathbf{u}\mathbf{u}}{\varepsilon}\right)}_{\text{convective term}} = -\underbrace{\frac{1}{\rho}\nabla(\varepsilon p)}_{\text{pressure term}} + \underbrace{\nu_e \nabla^2 \mathbf{u}}_{\text{Brinkman term}} - \underbrace{\frac{\nu\varepsilon}{K}\mathbf{u}}_{\text{Darcy term}} - \underbrace{\frac{\varepsilon C_F |\mathbf{u}|}{\sqrt{K}}\mathbf{u}}_{\text{Forchheimer term}} \tag{2}$$

where $\mathbf{u}$ is the local average velocity vector (Darcy velocity); ρ is the mass density of the fluid; p is the intrinsic-average pressure; ν is the fluid kinematic viscosity; ν_e is the effective (Brinkman) viscosity, which is set to be equal to ν in this paper; ε is the porosity; K is the permeability; and C_F is the geometric function that is expressed as [17]

$$C_F = 1.75/\sqrt{150\varepsilon^3}$$

The nonlinear Forchheimer term and linear Darcy term are drag forces caused by the presence of the porous medium. The Brinkman term accounts for the force due to the solid boundary. The local average p^* and the intrinsic average pressure p can be linked by the Dupuit–Forchheimer relationship $p^* = \varepsilon p$.

For steady incompressible viscous flow, the governing equations for a homogenous fluid region can be expressed as

$$\nabla \cdot \mathbf{u} = 0 \tag{3}$$

$$\nabla \cdot (\mathbf{u}\mathbf{u}) = -\frac{1}{\rho}\nabla p + \nu \nabla^2 \mathbf{u} \tag{4}$$

At the interface between the homogenous fluid layer and porous medium layer, additional boundary conditions must be applied to couple the flows in the two regions. In the present study, the stress jump condition [13] is applied

$$\frac{1}{\varepsilon}\frac{\partial u_t}{\partial n}\bigg|_{\text{porous}} - \frac{\partial u_t}{\partial n}\bigg|_{\text{fluid}} = \frac{\beta}{\sqrt{K}} u_t \bigg|_{\text{interface}} + \frac{\beta_1 u_t^2}{\nu} \tag{5}$$

where in the porous medium region, u_t is the Darcy velocity component parallel to the interface aligned with the direction t and normal to the direction n while in the homogenous fluid region u_t is the fluid velocity component parallel to the interface; β and β_1 are the stress jump parameters.

Ochoa-Tapia and Whitaker [13] derived analytical expressions for parameters β and β_1, which indicate their dependence on permeability and porosity. They concluded that these two parameters

DOI: 10.1002/fld

are both of order one. Ochoa-Tapia and Whitaker [12] experimentally determined that β varies from $+0.7$ to -1.0 for different materials with permeability varying from 15×10^{-6} to $127\times10^{-6}\,\text{in}^2$ and average pore size from 0.016 to 0.045 in. No experimental data are available for β_1. In the present study, both β and β_1 vary in the range from -1.0 to $+0.7$.

In addition to Equation (5), the continuity of velocity and normal stress prevailing at the interface is given by

$$\mathbf{u}|_{\text{fluid}}=\mathbf{u}|_{\text{porous}}=\mathbf{u}_{\text{int}} \tag{6}$$

$$\frac{v}{\varepsilon}\frac{\partial u_n}{\partial n}\bigg|_{\text{porous}}-v\frac{\partial u_n}{\partial n}\bigg|_{\text{fluid}}=0 \tag{7}$$

where in the porous medium region, u_n is the Darcy velocity component normal to the interface; and in the homogenous fluid region, u_n is the fluid velocity component normal to the interface; the subscript 'int' represents the interface. By combining with the appropriate boundary conditions of the composite region, Equations (1)–(7) can be used to simulate the flow in a system composed of a porous medium and a homogenous fluid.

3. LATTICE BOLTZMANN MODEL AND BOUNDARY CONDITIONS

3.1. Homogenous fluid region

In the LBM the fluid flow field is modeled by a single-particle DF f_i. The quantity of $f_i(\mathbf{x},t,\mathbf{e})$ represents the probability of finding a particle in the vicinity of $\mathbf{x}$ at time t that is moving with velocity $\mathbf{e}_i$. For the two-dimensional case, the lattice Boltzmann BGK equation is expressed as [16, 17, 20–23]

$$f_i(\mathbf{x}+\mathbf{e}_i\delta_t,t+\delta_t)-f_i(\mathbf{x},t)=-\frac{f_i(\mathbf{x},t)-f_i^{\text{eq}}(\mathbf{x},t)}{\tau} \tag{8}$$

where δ_t is the time increment, τ is the non-dimensional relaxation time and f_i^{eq} is the corresponding equilibrium state, which is the distribution that the system will evolve in the absence of forcing gradients. The EDF is defined by [17]

$$f_i^{\text{eq}}=w_i\rho\left[1+\frac{\mathbf{e}\cdot\mathbf{u}}{c_{\text{s}}^2}+\frac{\mathbf{uu}:(\mathbf{e}_i\mathbf{e}_i-c_{\text{s}}^2\text{I})}{2c_{\text{s}}^4}\right] \tag{9}$$

where w_i is the weight coefficient and c_{s} is the sound speed. Here $c_{\text{s}}=c/\sqrt{3}$, $c=\delta_x/\delta_t$ and δ_x is the lattice spacing. In present study, c is set to be 1. For the D2Q9 [17, 20, 21] model (Figure 1), the discrete velocities $(e_x,e_y)_i$ are defined as

$$\mathbf{e}_i=\begin{cases}(0,0), & i=0\\ (\cos[(i-1)\pi/2],\sin[(i-1)\pi/2]), & i=1,2,3,4\\ \sqrt{2}(\cos[(i-5)\pi/2+\pi/4],\sin[(i-5)\pi/2+\pi/4]), & i=5,6,7,8\end{cases} \tag{10}$$

DOI: 10.1002/fld

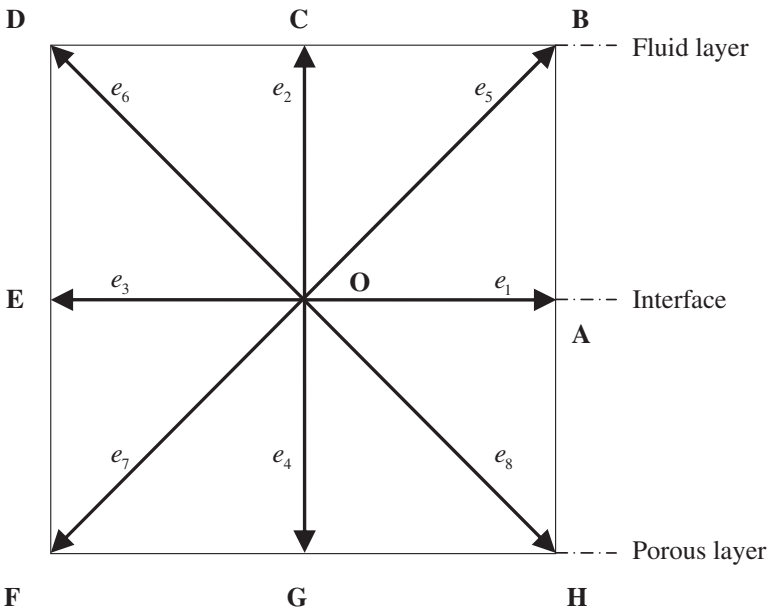

Figure 1. Basic lattice for the D2Q9 lattice Boltzmann model.

The weight coefficients are given as

$$w_i = \begin{cases} \frac{4}{9}, & i=0 \\ \frac{1}{9}, & i=1,2,3,4 \\ \frac{1}{36}, & i=5,6,7,8 \end{cases} \tag{11}$$

The macroscopic mass density ρ and velocity $\mathbf{u}$ are calculated from the DFs

$$\rho = \sum_{i=0}^{8} f_i, \quad \rho\mathbf{u} = \sum_{i=0}^{8} f_i \mathbf{e}_i \tag{12}$$

The pressure and the kinematic viscosity are defined as

$$p = \rho c_s^2, \quad v = c_s^2(\tau - \tfrac{1}{2})\delta_t \tag{13}$$

Using the Chapman–Enskog expansion [22], the momentum equation (4) can be recovered by performing a Taylor series expansion of the particle DF (8).

3.2. Porous medium region

To solve the porous medium flow governed by the Darcy–Brinkman–Forchheimer extended model (Equation (2)), Guo and Zhao [17] introduced the porosity into the EDF and added a force term

DOI: 10.1002/fld

F_i to the standard LBEs to account for the linear and nonlinear drag forces caused by the porous medium. Their model is expressed as

$$f_i(\mathbf{x}+\mathbf{e}_i\delta_t, t+\delta_t) - f_i(\mathbf{x}, t) = -\frac{f_i(\mathbf{x}, t) - f_i^{\mathrm{eq}}(\mathbf{x}, t)}{\tau} + \delta_t F_i \tag{14}$$

$$f_i^{\mathrm{eq}} = w_i \rho \left[1 + \frac{\mathbf{e}\cdot\mathbf{u}}{c_\mathrm{s}^2} + \frac{\mathbf{uu}:(\mathbf{e}_i\mathbf{e}_i - c_\mathrm{s}^2\mathrm{I})}{2\varepsilon c_\mathrm{s}^4} \right] \tag{15}$$

where the total force term F_i is defined by

$$F_i = w_i \rho \left(1 - \frac{1}{2\tau}\right) \left[1 + \frac{\mathbf{e}\cdot\mathbf{F}}{c_\mathrm{s}^2} + \frac{\mathbf{uF}:(\mathbf{e}_i\mathbf{e}_i - c_\mathrm{s}^2\mathrm{I})}{\varepsilon c_\mathrm{s}^4} \right] \tag{16}$$

where $\mathbf{F}$ is the total body force due to the presence of a porous medium and other external force fields; it is expressed as

$$\mathbf{F} = -\frac{\varepsilon v}{K}\mathbf{u} - \frac{\varepsilon C_\mathrm{F}}{\sqrt{K}}|\mathbf{u}|\mathbf{u} + \varepsilon\mathbf{g} \tag{17}$$

where $\mathbf{g}$ is the body force due to external force; and the fluid velocity is defined as

$$\rho\mathbf{u} = \sum_{i=0}^{8} \mathbf{e}_i f_i + \frac{\delta_t}{2}\rho\mathbf{F} \tag{18}$$

The nonlinear equation (18) was solved by Guo and Zhao [17] and expressed as

$$\mathbf{u} = \frac{\mathbf{v}}{c_0 + \sqrt{c_0^2 + c_1|\mathbf{v}|}} \tag{19}$$

where $\mathbf{v}$ is an auxiliary velocity defined as

$$\rho\mathbf{v} = \sum_{i=0}^{8} \mathbf{e}_i f_i + \frac{\delta_t}{2}\varepsilon\rho\mathbf{g} \tag{20}$$

The two parameters c_0 and c_1 in Equation (19) can be calculated by

$$c_0 = \frac{1}{2}\left(1 + \varepsilon\frac{\delta_t}{2}\frac{v}{K}\right), \quad c_1 = \varepsilon\frac{\delta_t}{2}\frac{C_\mathrm{F}}{\sqrt{K}} \tag{21}$$

Through the Chapman–Enskog expansion [17] the momentum equation (2) can be deduced from the DF (14).

3.3. Interfacial boundary condition treatment

The interfacial boundary condition must be chosen appropriately to couple the two LBEs as given by Equations (8) and (14). In the present study, the stress jump condition is used. For traditional discretization methods, such as finite-difference and finite-volume methods, the momentum flux is calculated by discretizing of the velocity field using finite difference. Thus the implementation of appropriate velocity boundary conditions automatically guarantees correct momentum flux near

DOI: 10.1002/fld

the boundary. However, in the LBM, only the equations for f_i are solved and the velocity boundary conditions are not enough to guarantee the strain field [24]. Thus additional boundary conditions for f_i must be correctly implemented to ensure correct momentum flux near boundary.

Figure 1 shows a basic lattice for D2Q9 lattice Boltzmann model with lattice layer (E–O–A) just at the interface, lattice layer (D–C–B) at one lattice inside of the fluid and lattice layer (F–G–H) at one lattice inside the porous medium. Consider the stress jump condition as a case, the normal velocity gradients at the interface can be calculated by using the backward second-order difference approximation for porous side and forward second-order difference approximation for fluid side:

$$\left.\frac{\partial u}{\partial y}\right|_{\text{porous}}=\frac{3u_{\text{int}}-4u_{\text{int}-1}+u_{\text{int}-2}}{2\Delta y},\quad \left.\frac{\partial v}{\partial y}\right|_{\text{porous}}=\frac{3v_{\text{int}}-4v_{\text{int}-1}+v_{\text{int}-2}}{2\Delta y} \tag{22}$$

$$\left.\frac{\partial u}{\partial y}\right|_{\text{fluid}}=\frac{-3u_{\text{int}}+4u_{\text{int}+1}-u_{int+2}}{2\Delta y},\quad \left.\frac{\partial v}{\partial y}\right|_{\text{fluid}}=\frac{-3v_{\text{int}}+4v_{\text{int}+1}-v_{\text{int}+2}}{2\Delta y} \tag{23}$$

where u_{int} is the interfacial velocity in x-coordinate; v_{int} is the interfacial velocity in y-coordinate; the subscript 'int' represents the lattice points at the interface, 'int-1' and 'int-2' represent the lattice points, which are one lattice and two lattices below the interface, respectively; 'int$+1$' and 'int$+2$' represent the lattice points, which are one lattice and two lattices above the interface, respectively; and Δy is the lattice spacing. By combining Equations (5), (7), (22) and (23)

$$\frac{1}{\varepsilon}\frac{3u_{\text{int}}-4u_{\text{int}-1}+u_{\text{int}-2}}{2\Delta y}\bigg|_{\text{porous}}-\frac{-3u_{\text{int}}+4u_{\text{int}+1}-u_{\text{int}+2}}{2\Delta y}\bigg|_{\text{fluid}}=\frac{\beta}{\sqrt{K}}u_{\text{int}}+\frac{1}{\nu}\beta_1 u_{\text{int}}^2 \tag{24}$$

$$\frac{1}{\varepsilon}\frac{3v_{\text{int}}-4v_{\text{int}-1}+v_{\text{int}-2}}{2\Delta y}\bigg|_{\text{porous}}-\frac{-3v_{\text{int}}+4v_{\text{int}+1}-v_{\text{int}+2}}{2\Delta y}\bigg|_{\text{fluid}}=0 \tag{25}$$

The interfacial velocities u_{int} and v_{int} can be calculated from Equations (24) and (25), respectively. Thus the interfacial boundary condition can be treated as the Dirichlet boundary condition (first type). In the present study, the Dirichlet boundary conditions are solved with the non-equilibrium extrapolation method that was proposed by Guo *et al.* [25]:

$$f_i(\mathrm{x}_{\text{int}})-\bar{f}_i^{\text{eq}}(\mathrm{x}_{\text{int}})=f_i(\mathrm{x}_f)-\bar{f}_i^{\text{eq}}(\mathrm{x}_f) \tag{26}$$

where x_{int} is a lattice node on the interfacial boundary and x_f is its nearest neighboring node along the discrete velocity e_i. That is, $\mathrm{x}_f=\mathrm{x}_{\text{int}}+\mathrm{e}_i\delta_t$; and the EDF at x_{int} is proposed as

$$\bar{f}_i^{\text{eq}}(\mathrm{x}_{\text{int}})=w_i\rho(\mathrm{x}_f)\left[1+\frac{e_i\cdot u(\mathrm{x}_{\text{int}})}{c_{\text{s}}^2}+\frac{u(\mathrm{x}_{\text{int}})u(\mathrm{x}_{\text{int}}):(e_ie_i-c_{\text{s}}^2\mathrm{I})}{2\varepsilon c_{\text{s}}^2}\right] \tag{27}$$

where $\rho(\mathrm{x}_f)$ is known and interfacial velocity $u(\mathrm{x}_{\text{int}})$ is calculated from Equations (24) and (25).

For channel flow with periodic boundary condition in inlet and outlet, the periodic boundary condition is applied to calculate f_1, f_5 and f_8 at the interface $f_{\text{in}1}=f_{\text{out}1}$, $f_{\text{in}5}=f_{\text{out}5}$ $f_{\text{in}8}=f_{\text{out}8}$; where the subscript 'in' and 'out' represent inlet and outlet, respectively. In the case of cavity

DOI: 10.1002/fld

flow, the no-slip boundary conditions are used for f_1, f_5 and f_8 at the left end of interface. Similar boundary conditions can be applied for the right end of the interface.

3.3.1. Calculation procedure

1. The computation of the flow field is started by assuming initial values for all the parameters.
2. The EDFs for the flow field, including those at the interface, are calculated. Then the collision step is carried out for all nodes, except the interfacial nodes where the velocity boundary conditions are enforced (in step 4) for the EDFs. After the collision step, the streaming step is executed for all nodes.
3. The macroscopic parameters, such as densities and velocities, are calculated from the updated DFs.
4. The jump conditions are implemented by using Equations (24) and (25) to calculate the updated interfacial velocities. The velocities and DF boundary conditions are enforced, including the updated interfacial velocities.
5. Convergence is checked by using the following condition:

$$\frac{\sum_{ij} |u_{ij}^{(n)} - u_{ij}^{(n-100)}|}{\sum_{ij} |u_{ij}^{(n)}|} \leqslant 10^{-9} \tag{28}$$

where $u_{ij}^{(n)} = u(x_i, y_j, n\Delta t)$. Equation (28) represents the sum of the non-dimensional error over total grid nodes. If Equation (28) is satisfied, the calculation is stopped and the results are outputted; if not, steps 2–5 are repeated till Equation (28) is satisfied.

4. RESULTS AND DISCUSSION

4.1. Channel flow partially filled with porous medium

The physical domain is shown schematically in Figure 2. It consists of a planar channel whose upper region of height H_1 is filled with homogenous fluid and lower region of height H_2 is filled

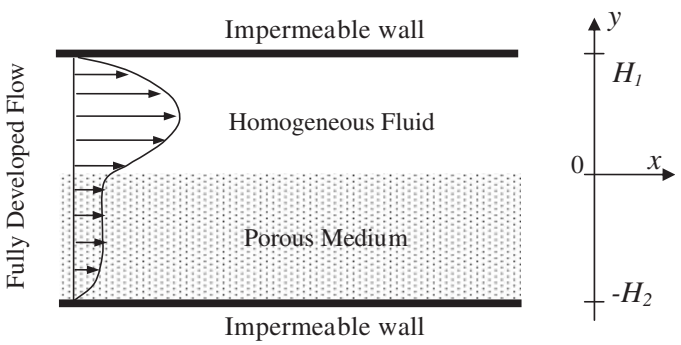

Figure 2. Schematic of flow in a channel partially filled with saturated porous medium.

DOI: 10.1002/fld

with a fluid-saturated porous medium region. A case of height ratio $H_2/H_1=1$ is considered. The flow is assumed laminar and the driving force is a constant pressure gradient.

There are several different ways to implement the driving force. In the present study, the driving force $G=-\mathrm{d}p_f/\mathrm{d}x$ is included in the lattice Boltzmann model by adding a first-order Hermite polynomials to the DFs [16, 21]:

$$\tilde{f}_i(\mathbf{x}_t,t)=f_i(\mathbf{x},t)+\frac{\omega_i G e_{ix}}{c_s^2} \quad \text{for homogenous fluid flow} \tag{29}$$

$$\tilde{f}_i(\mathbf{x}_t,t)=f_i(\mathbf{x},t)+\frac{\varepsilon\omega_i G e_{ix}}{c_s^2} \quad \text{for porous medium flow} \tag{30}$$

where $\tilde{f}_i(\mathbf{x}_t,t)$ represents the DF after including the driving force. The main dimensionless parameters are $U=\mu u/GH_1^2$, Darcy number $Da=K/H_1^2$ and $Y=y/H_1$. Both numerical and analytical solutions [15] are presented for validation of the present numerical implementation.

To guarantee grid-independent solution, a sufficiently fine mesh should be used. For the pressure-driven flow (Figure 2), the grid independence study (Figure 3) shows that a mesh of 121 grids in the y-direction is sufficient. For all of the channel flow cases in this paper, the driving force G is set to be 10^{-4}, and fluid kinematic viscosity v is set to be 2×10^{-3}. The grid independence study shows that the present results are in good agreement with the analytical results.

Figure 4(a)–(c) shows the velocity profiles at different *Da*, porosity and stress jump coefficient, respectively. The comparison shows that the present numerical results are in good agreement with the analytical solutions at various *Da*, porosities and stress jump coefficients. It is found that *Da* has much effect on the velocity profiles. The velocity increases significantly with increasing *Da* and proportionately more so for the porous side. The stress jump coefficient β has slight effect on the velocity profiles. The effect of the stress jump coefficient β_1 is negligible. This is attributed to the small Reynolds number and Darcy number. Thus the inertial effect is negligible, especially since the flow is parallel. The porosity has very little effect on the velocity profiles.

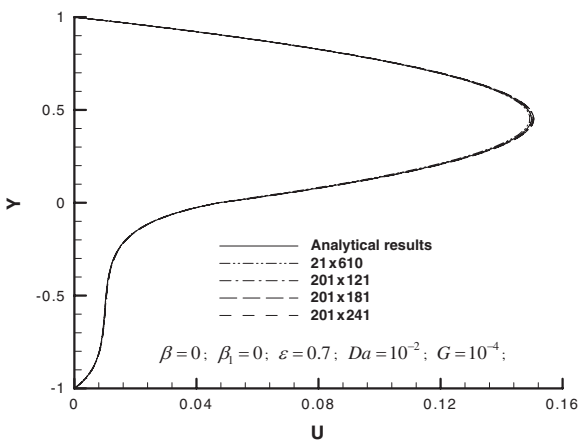

Figure 3. Effect of grid size on velocity profile.

DOI: 10.1002/fld

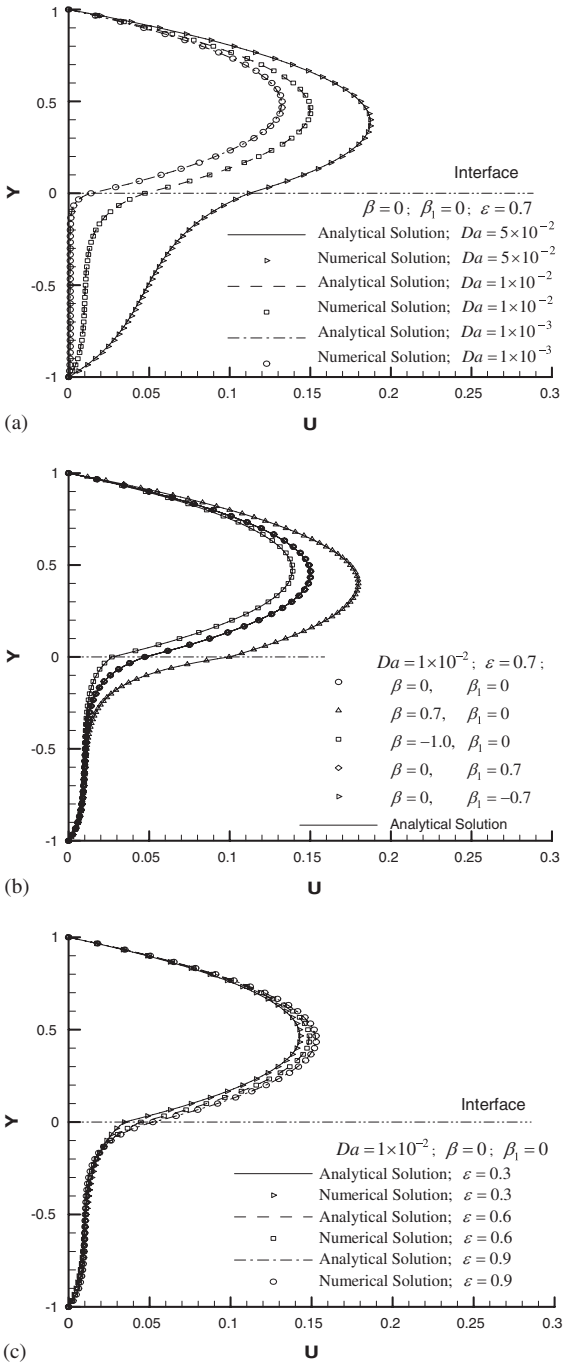

Figure 4. The u velocity profile under different flow conditions: (a) Darcy number effect; (b) stress jump coefficients β and β_1 effect; and (c) porosity effect.

DOI: 10.1002/fld

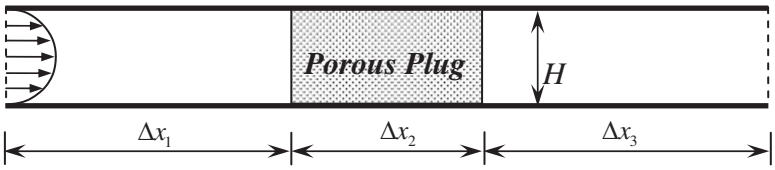

Figure 5. Schematic of flow in a channel with a porous plug.

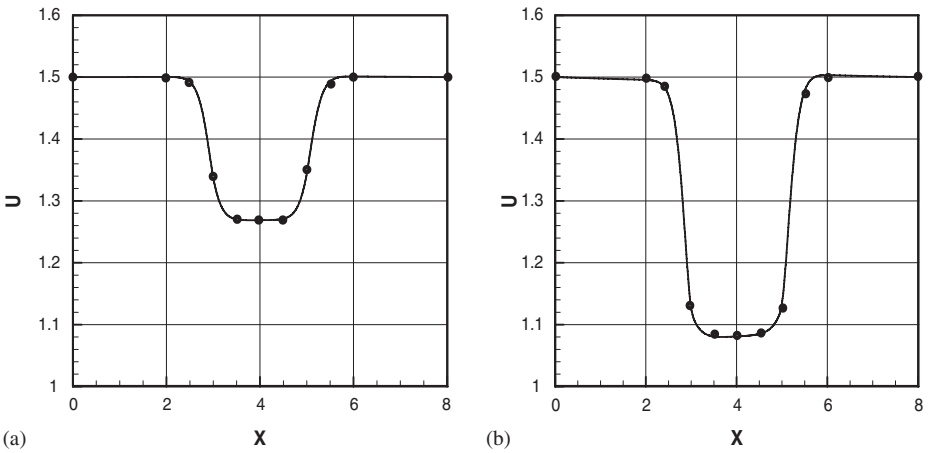

Figure 6. The velocity distributions along the centerline at (a) $Da=10^{-2}$ and (b) $Da=10^{-3}$; other parameters are $Re=1$, $\varepsilon=0.7$, $\beta=0$, $\beta_1=0$, $\Delta x1=\Delta x3=3H$ and $\Delta x2=2H$.

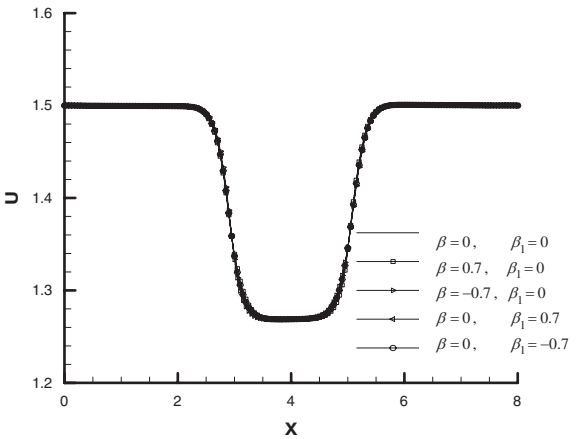

Figure 7. The velocity distribution along the centerline at different stress jump coefficients with $Da=10^{-2}$, $Re=1$, $\varepsilon=0.7$, $\Delta x_1=\Delta x_3=3H$ and $\Delta x_2=2H$.

DOI: 10.1002/fld

4.2. Flow through a channel with a porous plug

The physical domain of the flow through a channel with a porous plug is shown schematically in Figure 5, which is the same as that by Gartling *et al*. [26], Betchen *et al*. [27] and Yu *et al.* [15]. In this problem the dominating flow is perpendicular to the interface. Different from the first problem, the main dimensionless parameters are $U=u/u_a$, $X=x/H$, Reynolds number $Re=\rho u_a H/\mu$ and Darcy number $Da=K/H^2$, where u_a is the mean velocity. The Poiseuille flow velocity profile is set in the inlet based on the mean velocity.

The numerical results for the case of $Da=10^{-2}$ and 10^{-3} are shown in Figure 6, where the centerline U velocity along x-direction are presented. The other parameters for the flows illustrated in Figure 6 are $Re=1$, $\varepsilon=0.7$, $\beta=0$ and $\beta_1=0$. The lengths are set to be $\Delta x_1=\Delta x_3=3H$ and $\Delta x_2=2H$. In the present study, 121 grids in the y-direction are used and the preliminary numerical tests confirmed that the solutions are grid independent.

Figure 6 shows that the velocity drops rapidly in the porous plug, especially for the case with the low Darcy number. The flow field is predominantly axial over most of the homogenous fluid and porous medium regions, but it is two-dimensional in the region near the interface between the homogenous fluid and the porous medium. The present results are in good agreement with those of Gartling *et al*. [26], Betchen *et al*. [27] and Yu *et al.* [15].

The centerline velocity distributions at the different stress jump coefficients β and β_1 are shown in Figure 7. It is seen that the two coefficients have negligible effects as the dominant flow direction is perpendicular to the interface. The present results agree well with those of previous studies [15, 26, 27].

4.3. Lid-driven cavity flow partially filled with porous medium

Figure 8 is the schematic diagram of flow in a lid-driven square cavity, which is three-quarter filled with porous medium. The fluid kinematic viscosity v is set to be 2×10^{-3}. The governing

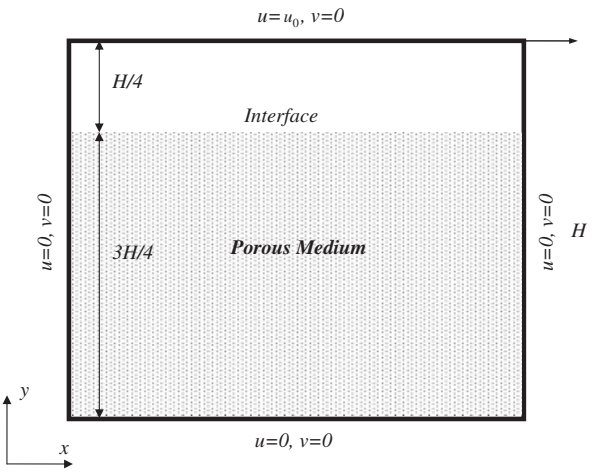

Figure 8. Schematic of flow in a square cavity partially filled with porous medium.

DOI: 10.1002/fld

dimensionless parameters are Reynolds number based on lid velocity u_0, $Re=u_0H/v$ and is given as a constant, Darcy number $Da=K/H^2$, $U=u/u_0$, $V=v/u_0$, $X=x/H$ and $Y=y/H$, where H is the square cavity height. The lid velocity u_0 can be calculated from the definition of Reynolds number. The mesh size of 121×121 is used, based on the previous grid independence studies. The stress jump conditions are implemented for x-component velocity U as given in Equation (5). And the stress continuity conditions are used for y-component velocity V as given in Equation (7).

Figure 9(a) and (b) shows the velocity profiles at different Da. It can be seen that there is more flow passing through the porous medium region with larger Darcy number. The interfacial velocity V increases with increasing Da. It shows that Darcy number has much effect on velocity profiles.

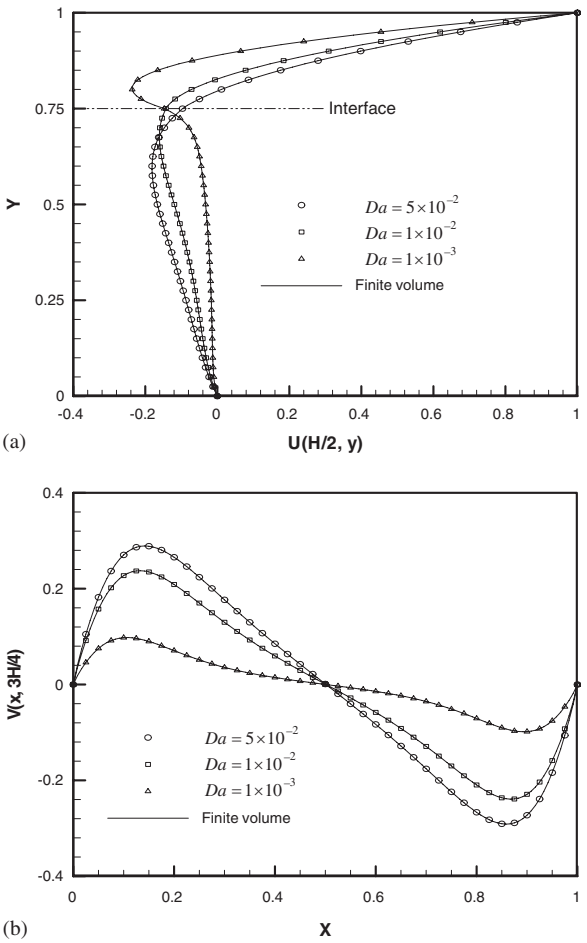

Figure 9. Velocity profiles at different Darcy number; symbols represent LBM solutions and solid lines represent finite-volume solutions: (a) centerline velocity U along y-direction and (b) interfacial velocity V along x-direction; other parameters are $Re=1$, $\varepsilon=0.7$, $\beta=0$ and $\beta_1=0$.

DOI: 10.1002/fld

The comparison shows that the present results are in good agreement with the finite-volume results.

The velocity profiles at different porosity are shown in Figure 10(a) and (b). It shows that porosity has very slight effects on velocity profiles. Figure 11(a) and (b) shows the velocity profiles at different stress jump coefficients. It can be seen that jump coefficient β has slight effect on the x-component velocity U. However, it has negligible effect on the y-component velocity V. The effect of the jump coefficient β_1 is negligible for both U and V. This may be due to the reason that for small Reynolds number and Darcy number used in present study, the inertial effects are negligible.

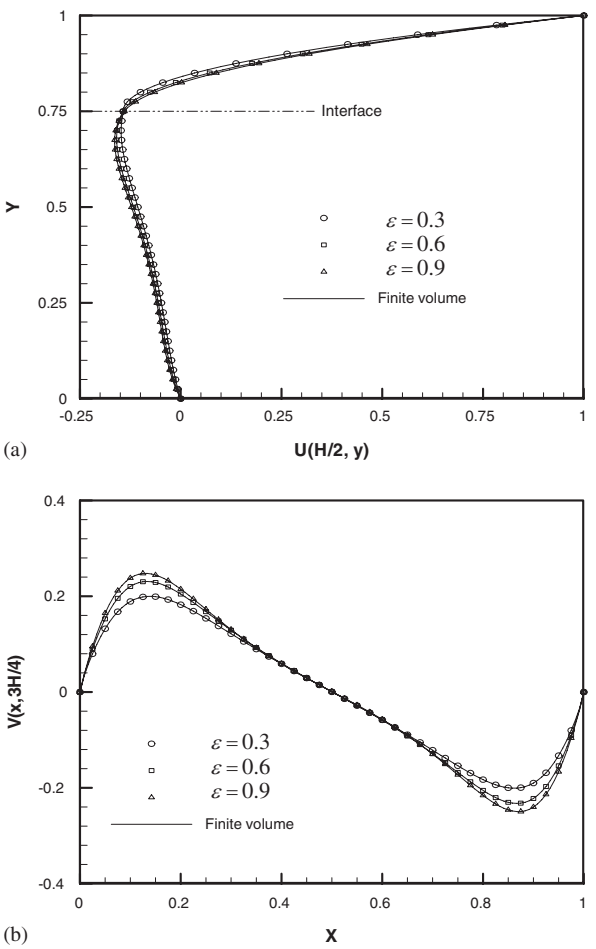

Figure 10. Velocity profiles at different porosity; symbols represent LBM solutions and solid lines represent finite-volume solutions: (a) centerline velocity U along y-direction and (b) interfacial velocity V along x-direction; other parameters are $Re=1$, $Da=10^{-2}$, $\beta=0$ and $\beta_1=0$.

DOI: 10.1002/fld

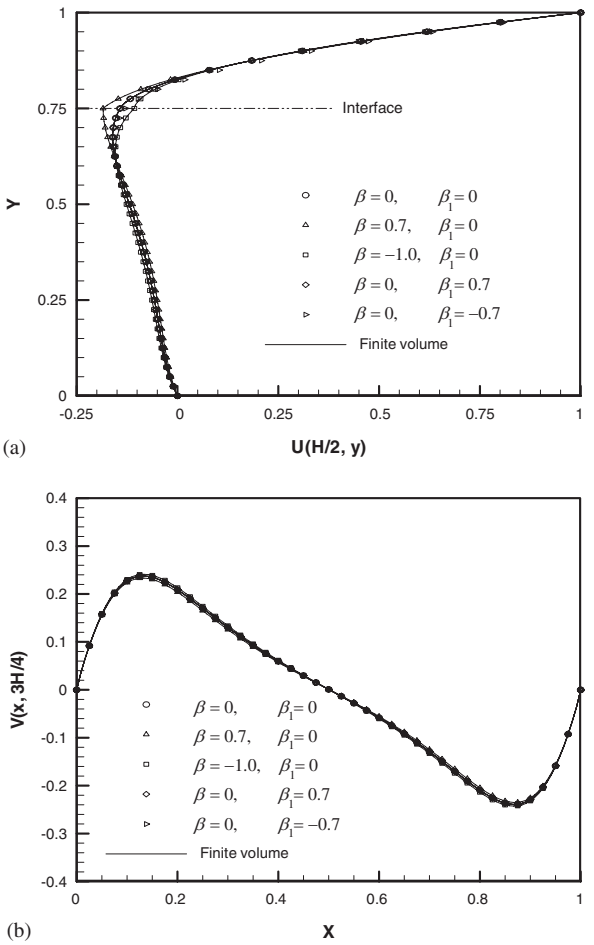

Figure 11. Velocity profiles at different stress jump coefficients; symbols represent LBM solutions and solid lines represent finite-volume solutions: (a) centerline velocity U along y-direction and (b) interfacial velocity V along x-direction; other parameters are $Re = 1$, $\varepsilon = 0.7$ and $Da = 10^{-2}$.

5. CONCLUSION

In this paper the LBE was extended to flow systems with regions of homogenous fluid and porous medium coupled by the stress jump interfacial boundary condition of Ochoa-Tapia and Whitaker [11–13]. A treatment of the velocity functions and DFs at the interface was described. The interfacial velocity was calculated with the difference approximation of the velocity gradient derivatives in the stress jump condition. Then the updated interfacial velocity was used to update the DFs at the interface.

This interfacial treatment was applied to simulate coupled flow problems such as channel flow, porous plug and cavity flow. These cases cover a variety of situations where the major flow is

DOI: 10.1002/fld

parallel, perpendicular and oblique to the interface. The stress jump parameter β has more effect when the velocity is parallel to the interface. The results are in consistent with the analytical and/or finite-volume results.

REFERENCES

1. Mercier J, Weisman C, Firdaouss M, Quéré PL. Heat transfer associated to natural convection flow in a partly porous cavity. *ASME Journal of Heat Transfer* 2002; **124**:130–143.
2. Jue TC. Numerical analysis of vortex shedding behind a porous cylinder. *International Journal of Numerical Methods for Heat and Fluid Flow* 2004; **14**:649–663.
3. Silva RA, de Lemos MJS. Numerical analysis of the stress jump interface condition for laminar flow over a porous layer. *Numerical Heat Transfer A* 2003; **43**:603–617.
4. Costa VAF, Oliveira LA, Baliga BR, Sousa ACM. Simulation of coupled flows in adjacent porous and open domains using a control-volume finite-element method. *Numerical Heat Transfer A* 2004; **45**:675–697.
5. Goyeau B, Lhuillier D, Gobin D, Velarde MG. Momentum transport at a fluid-porous interface. *International Journal of Heat and Mass Transfer* 2003; **46**:4071–4081.
6. Nield DA. Discussion. *ASME Journal of Heat Transfer* 1997; **119**:193–194.
7. Beavers GS, Joseph DD. Boundary conditions at a natural permeable wall. *The Journal of Fluid Mechanics* 1967; **30**:197–207.
8. Neale G, Nader W. Practical significance of Brinkman's extension of Darcy's law: coupled parallel flows within a channel and a bounding porous medium. *Canadian Journal of Chemical Engineering* 1974; **52**:475–478.
9. Vafai K, Kim SJ. Fluid mechanics of the interface region between a porous medium and a fluid layer—an exact solution. *International Journal of Heat and Fluid Flow* 1990; **11**:254–256.
10. Kim SJ, Choi CY. Convection heat transfer in porous and overlying layers heated from below. *International Journal of Heat and Mass Transfer* 1996; **39**:319–329.
11. Ochoa-Tapia JA, Whitaker S. Momentum transfer at the boundary between a porous medium and a homogeneous fluid I: theoretical development. *International Journal of Heat and Mass Transfer* 1995; **38**:2635–2646.
12. Ochoa-Tapia JA, Whitaker S. Momentum transfer at the boundary between a porous medium and a homogeneous fluid II: comparison with experiment. *International Journal of Heat and Mass Transfer* 1995; **38**:2647–2655.
13. Ochoa-Tapia JA, Whitaker S. Momentum jump condition at the boundary between a porous medium and a homogeneous fluid: inertial effect. *Journal of Porous Media* 1998; **1**:201–217.
14. Alazmi B, Vafai K. Analysis of fluid flow and heat transfer interfacial conditions between a porous medium and a fluid layer. *International Journal of Heat and Mass Transfer* 2001; **44**:1735–1749.
15. Yu P, Lee TS, Zeng Y, Low HT. A numerical method for flows in porous and homogenous fluid domains coupled at the interface by stress jump. *International Journal for Numerical Methods in Fluids* 2007; **53**:1755–1775.
16. Martys NS. Improved approximation of the Brinkman equation using a lattice Boltzmann method. *Physics of Fluids* 2001; **13**:1807–1810.
17. Guo Z, Zhao TS. Lattice Boltzmann model for incompressible flows through porous media. *Physical Review E* 2002; **66**:036304.
18. Pan C, Prins JF, Miller CT. A high-performance lattice Boltzmann implementation to model flow in porous media. *Computer Physics Communications* 2004; **158**:89–105.
19. Wang J, Zhang X, Bengough AG, Crawford JW. Domain-decomposition method for parallel lattice Boltzmann simulation of incompressible flow in porous media. *Physical Review E* 2005; **72**:016706.
20. Hou S, Zou Q, Chen S, Doolen GD, Cogley AC. Simulation of cavity flow by the lattice Boltzmann method. *Journal of Computational Physics* 1995; **118**:329–347.
21. Guo Z, Zheng C, Shi B. Discrete lattice effects on the forcing term in the lattice Boltzmann method. *Physical Review E* 2002; **65**:046308.
22. Guo Z, Zhao TS, Shi Y. Preconditioned lattice-Boltzmann method for steady flows. *Physical Review E* 2004; **70**:066706.
23. Shi Y, Zhao TS, Guo Z. Lattice Boltzmann method for incompressible flows with large pressure gradients. *Physical Review E* 2006; **73**:026704.
24. Chen S, Martinez D, Mei R. On boundary conditions in lattice Boltzmann methods. *Physics of Fluids* 1996; **8**(9):2527–2536.
25. Guo Z, Zheng C, Shi B. An extrapolation method for boundary conditions in lattice Boltzmann method. *Physics of Fluids* 2002; **14**:2007–2010.

DOI: 10.1002/fld

26. Gartling DK, Hickox CE, Givler RC. Simulation of coupled viscous and porous flow problems. *Computational Fluid Dynamics* 1996; **7**:23–48.
27. Betchen L, Straatman AG, Thompson BE. A nonequilibrium finite-volume model for conjugate fluid/porous/solid domains. *Numerical Heat Transfer A* 2006; **49**:543–565.

DOI: 10.1002/fld